Research Article | Vol. 27, No. 8 | 15 Apr 2019 | OPTICS EXPRESS 11651
Optics EXPRESS

Improved bandwidth of open loop liquid crystal adaptive optics systems with a proportional-derivative controller

XINGYUN ZHANG,[1] ZHAOLIANG CAO,[2] CHENGLIANG YANG,[1] ZENGHUI PENG,[1] QUANQUAN MU,[1,3,*] AND LI XUAN[1]

[1]*State Key Laboratory of Applied Optics, Changchun Institute of Optics, Fine Mechanics and Physics, Chinese Academy of Sciences, Changchun, Jilin 130033, China*
[2]*School of Mathematics & Physics, Suzhou University of Science and Technology, Suzhou, Jiangsu 215009, China*
[3]*Center of Materials Science and Optoelectronics Engineering, University of Chinese Academy of Sciences, Beijing 100049, China*
**muquanquan@ciomp.ac.cn*

Abstract: Open loop liquid crystal adaptive optics (LC AO) has overcome the disadvantage of low energy efficiency after years of research, and its use is very promising in ground-based large aperture telescopes for visible band imaging. However, the low system bandwidth of open loop LC AO still limits its application. In order to solve this problem, we bring the concept of proportional-derivative control (which is widely used in closed loop systems) into open loop LC AO in this paper. Experiment results verified that the system −3 dB rejection bandwidth could improve from 75 Hz to 112 Hz when tip-tilt aberration is introduced, and the mean relative contrast ratio of imaging results could improve 80% when high-order aberrations are introduced. The proposed control method has significant meaning in promoting the application of open loop LC AO in ground-based large aperture telescopes for visible imaging.

1. Introduction

Adaptive optics (AO) could compensate the wavefront distortion caused by Earth's atmosphere turbulence in real time, hence it could tremendously improve the resolution of ground-based optical telescopes. Normally, deformable mirror (DM) is used as the wavefront corrector of AO systems. However limited by the manufacturing technology, the actuator number of DM couldn't reach very high (thousands at the current state of art). Hence so far most DM AO work in the 1-2.5 um wavelength range (the NIR) rather in the visible (λ < 1 um, where AO would require much more actuators). While visible AO has many scientific advantages over the NIR: better science detectors, much darker skies, strong emission lines, off the Rayleigh-Jeans tail, higher spatial resolution [1]. Recently, a few visible AO have been reported, like Robo-AO [2], MagAO [1] and SPHERE/ZIMPOL [3]. SPHERE/ZIMPOL is the largest (8 m telescope), which use a DM with 1681 (1377 active) actuators. Limited by actuators, DM is hardly possible to be used in visible AO for next generation extremely large telescopes(like TMT [4] and ELTs [5]), which would require at least ten times more actuators.

Due to the birefringence property, nematic liquid crystal (LC) is convenient to realize phase modulation [6]. So LC becomes a delightful material to make wavefront correctors. Furthermore, thanks to its applications in display industry, LC has the advantages of low driving voltage (10 V) and easy to reach millions of pixels [7], so liquid crystal wavefront corrector (LCWC) has the potentiality to be used in visible band AO for large aperture telescopes, and has been investigated in recent years [8–10]. However liquid crystal adaptive

#358059 https://doi.org/10.1364/OE.27.011651
Journal © 2019 Received 21 Jan 2019; revised 20 Mar 2019; accepted 20 Mar 2019; published 12 Apr 2019

Optics EXPRESS

optics (LC AO) still has disadvantages of low energy efficiency and low system bandwidth, which limits its application to ground-based large aperture telescopes.

Energy efficiency is crucial for an AO system, it in a large part determines how dark a target the system could observe. Since LCWC is polarization-dependent and has a relatively narrow working waveband (about 200 nm), so the energy utilization ratio of LC AO would be very low. Love [11,12] and Stockley [13] have proposed some methods to improve the energy efficiency of LCWC, but these methods also have disadvantages like decline in response speed, fabrication difficulty or amplitude modulation. Our working group proposed a novel energy-splitting optical design based on open loop control scheme [14–16]: the waveband of 400-700 nm is split for wavefront detection, and the 700-900 nm waveband is split for imaging after corrected by two LCWCs (each LCWC cope with one polarized beam: P and S). In this case, the whole 400-900 nm waveband of light could be fully utilized, so the energy efficiency problem of LC AO is solved.

System bandwidth is another crucial requirement for an AO system, it directly limits how violent the turbulence the system could cope with. And the time delay of hardware is a major factor that limits system bandwidth. Our working group has done many fruitful researches in reducing time delays of LC AO: the response time of LC has reduced from tens of milliseconds to less than 1 millisecond by synthesizing high birefringence and low viscosity materials and driving with overdriving technique [17]; and the data processing time has reduced to less than 0.2 ms by a symmetrical algorithm [18] with graphics processing unit (GPU). With those efforts, we have improved the −3 dB rejection bandwidth of LC AO to 70 Hz. Which is still not enough to cope with extreme turbulence conditions, since the Greenwood frequency of atmospheric turbulence could exceed 100 Hz in such conditions. As for DM AO, There have been reports about system bandwidth more than 100 Hz [19,20].

With certain hardware conditions, the bandwidth of an AO system is mainly determined by the controller of the system. While open loop control scheme brings great benefits in energy efficiency for LC AO, it also causes huge difficulties in controller design at the same time. Since in an open loop system, the sensor won't be able to measure the system residual error, so there won't be any feedback to the controller. Normally, open loop LC AO adopts a simple proportional controller, which has limited performance in improving system bandwidth.

In order to improve system bandwidth, we bring the concept of proportional-derivative control (which is widely used in closed loop systems) into open loop LC AO in this paper. In Section 2, we introduce the principles of open loop LC AO. Section 3 describes the control algorithm we proposed, and Section 4 presents the experimental results. Finally the conclusions are drawn in Section 5.

2. Principles of open loop LC AO

The principles of a typical open loop LC AO is shown in Fig. 1. The system is mainly comprised of five major devices: a Shack-Hartmann Wavefront Sensor (WFS) to measure the distorted wavefront in real time, a Tip-Tilt Mirror (TTM) to correct the tip-tilt part of the distorted wavefront, a Liquid Crystal Wavefront Corrector (LCWC) to correct the high-order aberrations, a Scientific CCD for imaging, and a Control Computer (CC) to mobilize all these devices. Apparently, TTM is located 'before' WFS, so WFS could measure the tip-tilt correction residuals of TTM and feeds back to CC. Then TTM, WFS and CC form a closed loop system, which is not the interest of this paper. While LCWC is placed 'after' or 'parallel' to WFS, therefore WFS won't be able to measure the high-order correction residuals of LCWC, which means there won't be any feedback for the control of LCWC. So LCWC, WFS and CC form an open loop system, which is exactly the topic of this article. The 'open loop LC AO' referred in this article are all targeted to this system.

Optics EXPRESS

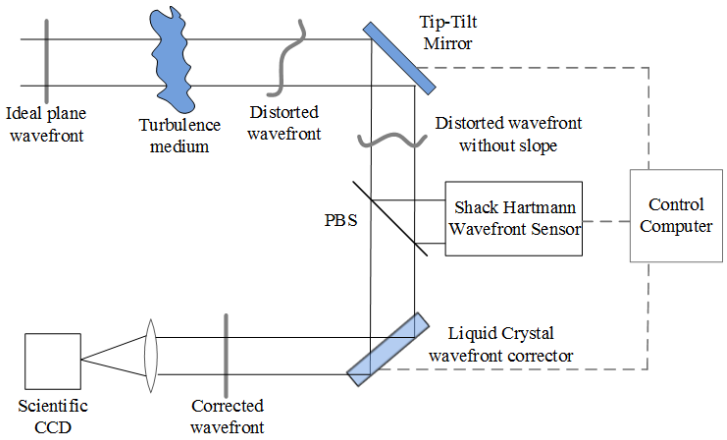

Fig. 1. Schematic diagram of open loop LC AO.

The control diagram of open loop LC AO is shown in Fig. 2. Where $\boldsymbol{\Phi}_t$ represents the turbulence wavefront, u is the aberration measured by WFS, y is the output of the controller (CC), and $\boldsymbol{\Phi}_c$ is the correcting wavefront generated by LCWC, the wavefront after correction (with residual error e) is imaged with CCD.

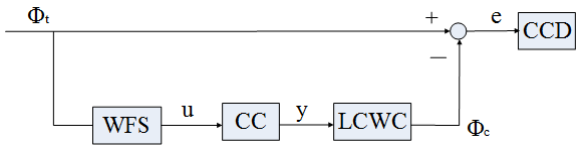

Fig. 2. Control diagram of open loop LC AO.

We have built a LC AO system with parameters as follows: a WFS which has 400 (20 × 20) micro-lens, 120 × 120 pixels, 1562 Hz frame rate, and 0.37 ms readout time; a LCWC which has 256 × 256 pixels, a response time of 0.64 ms and a data transmission time of 0.12 ms; a Andor DU888 CCD with 1024 × 1024 pixels; the wavefront reconstruction adopts 170 Zernike modes; and data processing takes 0.2 ms. And the whole system works as the following time sequence shown in Fig. 3, where WFS works in frame transfer mode. This system is designed for a 2 m telescope for visible imaging, and will be mounted for space observation in the following year.

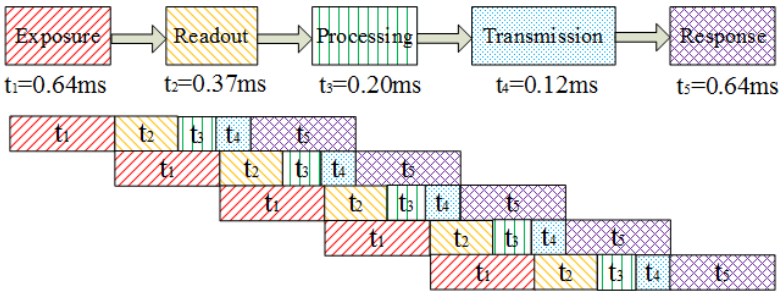

Fig. 3. The time sequence of the open loop LC AO.

With the system modeling method brought up in [21], we identified the system transfer function of this system as shown in Eq. (1), which describes the relationship between system

Optics EXPRESS

output and system input, and also represents the z-transfer of system's impulse response with all initial conditions assumed to be zero (where z is the shift operator).

$$G_o(z) = \frac{0.116z^{-1} + 0.412z^{-2}}{1 - 0.720z^{-1} + 0.207z^{-2}} \quad (1)$$

As described in Section 1, open loop LC AO normally adopts a simple proportional controller, as shown in Eq. (2). With the system model described above, we could conveniently simulate the performances of LC AO under different proportional controllers.

$$y(n) = P * u(n) \quad (2)$$

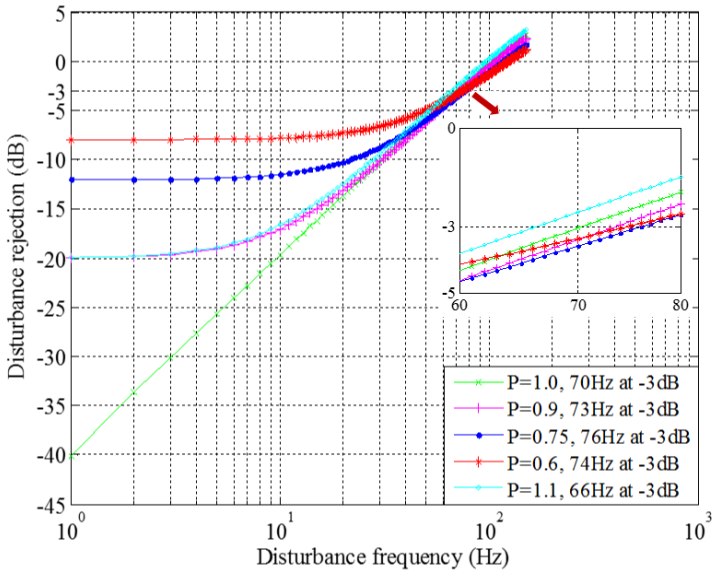

Fig. 4. Performances of LC AO with different proportional controllers.

As we can see from Fig. 4, when the ***P*** parameter of proportional controller takes 1.0, LC AO has the best ability to reject disturbance in low frequency and a −3 dB rejection bandwidth of 70 Hz. And −3 dB bandwidth could reach to about 76 Hz by adjusting parameter ***P***, while in the meantime the performance would considerably decline in low frequency. So proportional controller is not suitable for improving the system bandwidth of open loop LC AO.

3. Proportional-derivative control for open loop LC AO

Proportional-Integral-Derivative (PID) control in widely used in closed loop systems, for its effectiveness, simplicity and robust. While Integral element is only efficient when the input to the controller is residual error (exclusive for closed loop systems), so we bring the concept of proportional-derivative control into open loop LC AO, as shown in Eq. (3). With a proportional element to guarantee the system performance in low frequency, and a derivative element to improve the system performance in high frequency. The input u of the controller is the uncorrected aberration measured by WFS, differs from the residual error for that of closed loop AO.

$$y(n) = P * u(n) + D * [u(n) - u(n-1)] \quad (3)$$

In fact, the derivative element is a ***D***-step prediction of the aberration, so the parameter ***D*** is determined by the total time delay t_d of the system, as shown in Eq. (4). Where $t_d = t_1/2 + t_2 + t_3 + t_4 + t_5/2$, and t_1, t_2, t_3, t_4, t_5 are time of WFS exposure, WFS readout, data processing,

data transmission and LCWC response respectively as shown in Fig. 3. Only half of t_1 and t_5 is taken into account, since technically they are not pure time delay.

$$D = t_d / t_1 \tag{4}$$

In our LC AO system, D is about 2.0. And the parameter P should be set close to 1.0 to guarantee the system performance in low frequency. The performances of the proposed proportional-derivative controller is also simulated with the system model shown in Eq. (1). As shown in Fig. 5, simulation results meet our expectations perfectly: The derivative element significantly improves the system performance in high frequency (best results at D = 2.0), and the proportional element guarantees the system performance in low frequency (best results at P = 1.0). However, due to the influence of measuring noise, a rejection below –20 dB is normally hard to achieve in practice. Therefore weighed up the system performance in low and high frequency, we finally select P = 0.9 and D = 2.0.

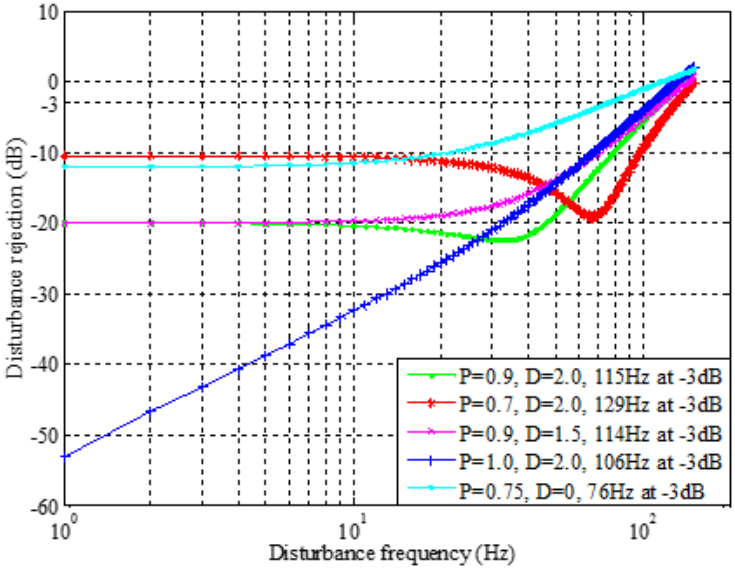

Fig. 5. Performances of LC AO with proportional-derivative controllers.

4. Experimental results

4.1. –3 dB rejection bandwidth of open loop LC AO

It is difficult to measure the rejection of high order aberrations, the tip-tilt rejection could be easily measured [22]. Moreover, the phase modulation of LCWC is achieved with the rotation of liquid crystal molecules, no mechanical motion is involved in such process, so for LCWC there is no difference between tip-tilt and high order aberrations in response characteristics. Therefore we could test the system rejection bandwidth for tip-tilt aberration, and assume it's also efficient for high order aberrations, like what was done by Dayton [22]. The schematic diagram of the laboratory layout is shown in Fig. 6. A xenon lamp is used as the light source, MS is a 700-900 nm narrow-band spectral filter with central wavelength at 785 nm. Tip-Tilt Mirror (TTM) is used to generate tip-tilt aberrations in different frequencies (f = 5, 10 … 120 Hz), which are measured by Hartmann wavefront sensor (WFS) as the input of the controller. Then liquid crystal wavefront corrector (LCWC) is driven by the output of the controller to compensate those aberrations, and the residual error is measured by another Hartmann wavefront sensor (WFS2). The disturbance rejection in deci-Bells (dB) is defined in the following Eq. (5), and the –3 dB rejection bandwidth is the frequency where half the

Optics EXPRESS

disturbance power is rejected by the system, i.e. the calculation of Eq. (5) is equal to −3 dB [22].

$$rej(dB) = 20\log_{10}(\frac{OutputDisturbanceAmplitude}{InputDisturbanceAmplitude}) \quad (5)$$

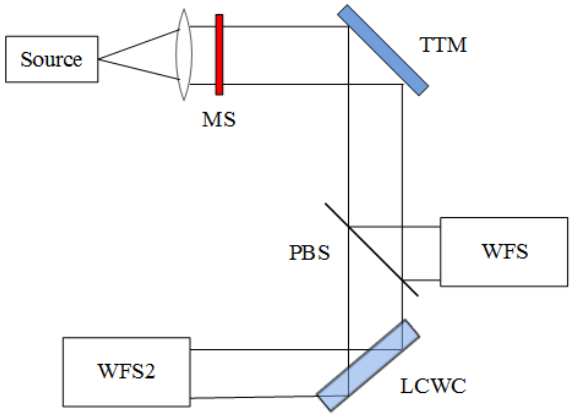

Fig. 6. Schematic diagram of the laboratory layout to measure system bandwidth.

As shown in Fig. 7, Experimental results match perfectly with simulations. The proposed proportional-derivative controller could improve disturbance rejection bandwidth from 75 Hz to 112 Hz, with much better rejection in low frequency (blow −15 dB from 0 to 55 Hz) at the same time.

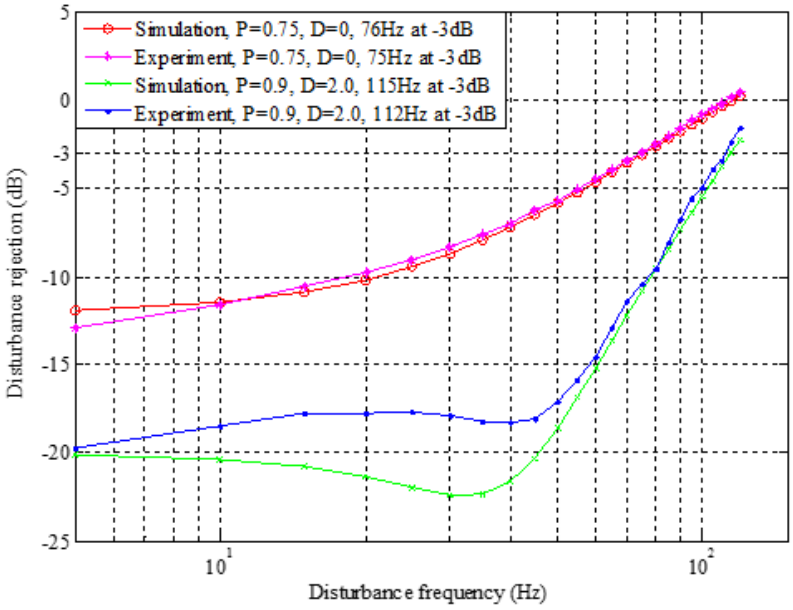

Fig. 7. System bandwidth measured in experiment.

4.2. Imaging results of open loop LC AO

In Section 4.1, we confirm that with P-D controller the system −3 dB rejection bandwidth could improve from 75 Hz to 112 Hz when tip-tilt aberration is introduced. In order to further verify the performance of our proposed controller for high order aberrations, we design an

Optics EXPRESS

imaging experiment setup as shown in Fig. 8. A xenon lamp is used as the light source, and a resolution target is placed as the imaging target (the red circle in Fig. 8 is the illuminating area). The angular separation between the fifth line pair of the fourth group is about 200 mas (correspond to 2 times the diffraction limit of the 2 m telescope). It is the designed goal resolution of our LC AO, for the consideration of both imaging resolution and field of the scientific CCD (Andor DU888). MS is a 700-900 nm narrow-band spectral filter with central wavelength at 785 nm.

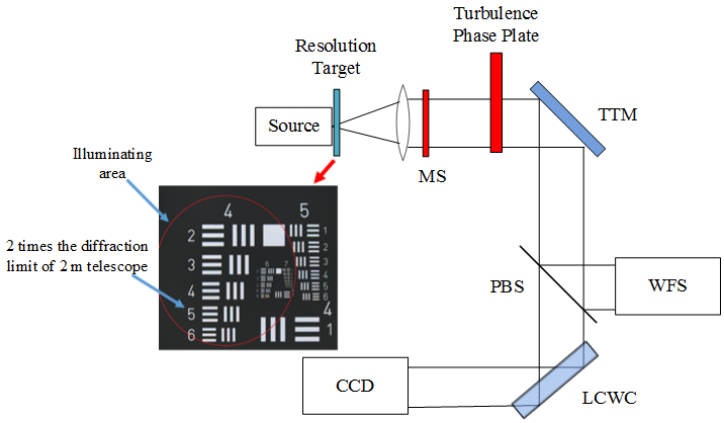

Fig. 8. Schematic diagram of the imaging experiment setup.

And a turbulence phase plate (Lexitek Inc) is put in the system to introduce turbulence aberration. As shown in Fig. 9, the surface of the phase plate is machined with the design optical path difference, and when the phase plate rotates driven by an electromotor, the light spot will scan different areas of the plate. Then a dynamic aberration will be introduced into the system and it obeys the Kolmogorov power law but is periodic. By adjusting the beam diameter of the light spot and the rotational speed of the plate, the atmospheric coherence length $\mathbf{r_0}$ and Greenwood frequency of the introduced aberration is tunable.

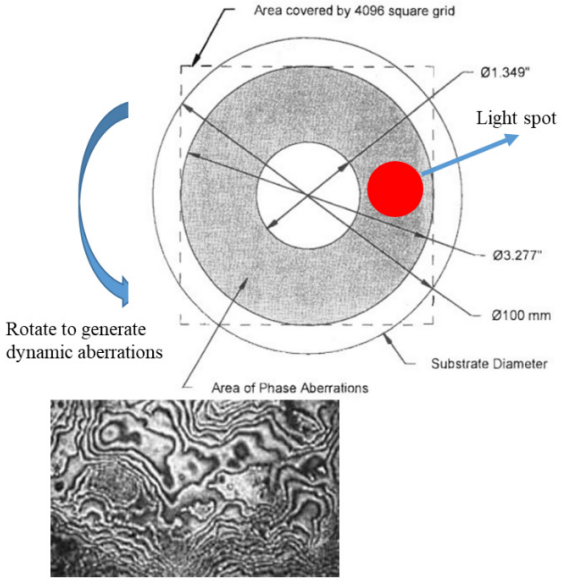

Fig. 9. Lexitek's turbulence phase plate.

Optics EXPRESS

We test the performance of our proposed controller under a turbulence aberration with Greenwood frequency of about 100Hz, atmospheric coherence length of about 10 cm (at 550 nm wavelength) and amplitude of about 10 um. The tip-tilt part of the aberration is corrected by TTM in closed loop, and 2-170th Zernike modes of the high order aberrations are corrected by LCWC in open loop with both Proportional controller and P-D controller. We confirm that Proportional controller has the best performance when $\boldsymbol{P}$ = 0.75, and P-D controller has the best performance when $\boldsymbol{P}$ = 0.9 and $\boldsymbol{D}$ = 2.0. And the comparison between those two controllers are shown in Fig. 10. Since the introduced aberration is periodic, we could think those two controllers are working on the same turbulence condition. The image before AO correction is shown in Fig. 10(a). And Fig. 10(b) is the video (see Visualization 1) after AO correction, where the first half is corrected with Proportional controller ($\boldsymbol{P}$ = 0.75) and the remaining half is corrected with P-D controller ($\boldsymbol{P}$ = 0.9, $\boldsymbol{D}$ = 2.0). In best cases the imaging qualities are good for both proportional controller in Fig. 10(d) and P-D controller in Fig. 10(f). However, in worst cases the fifth line pair would be hardly distinguishable for proportional controller in Fig. 10(c), while it could be clearly distinguished for our proposed P-D controller in Fig. 10(e).

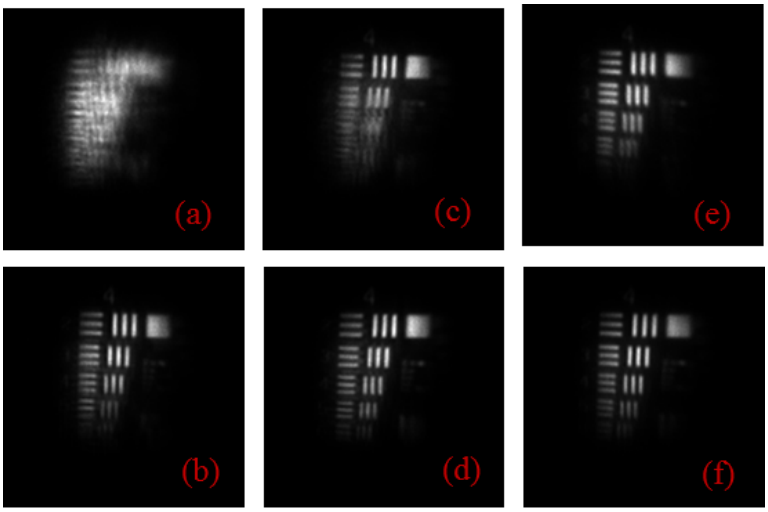

Fig. 10. Imaging result. (a) Before AO correction; (b) After AO correction, (see Visualization 1) first half Proportional controller and the remaining half P-D controller; (c) Worst and (d) best result after AO correction with Proportional controller; (e) Worst and (f) best result after AO correction with P-D controller.

In order to assess the imaging quality visually, we define the relative contrast ratio ($\boldsymbol{C_r}$) between light intensity of the bright ($\boldsymbol{I_b}$) and dark ($\boldsymbol{I_d}$) fringe of the fifth line pair of the fourth group as Eq. (6). The bigger $\boldsymbol{C_r}$ the more distinguishable of the line pair, and it would be totally undistinguishable when $\boldsymbol{C_r}$ is 0. Figure 11 shows the $\boldsymbol{C_r}$ value of each single frame of the video in Visualization 1, the mean relative contrast ratio increases from 0.60 to 1.08 with our proposed P-D controller.

$$C_r = (I_b - I_d) \Big/ I_d \tag{6}$$

Optics EXPRESS

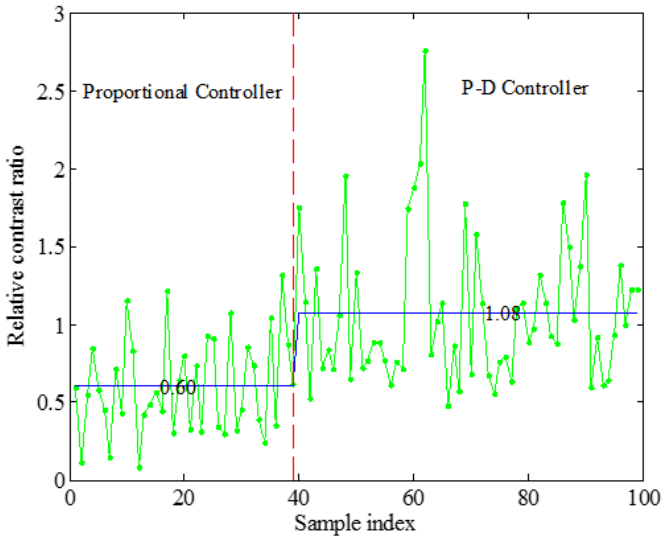

Fig. 11. Comparison of the relative contrast ratio.

5. Conclusions

In this paper, we proposed a proportional-derivative controller for open loop liquid crystal adaptive optics (LC AO). Both simulation and experiment showed extremely great benefits in improving system bandwidth and guaranteeing good performance in low frequency at the same time. The system −3 dB rejection bandwidth could improve from 75 Hz to 112 Hz when tip-tilt aberration was introduced, and the mean relative contrast ratio of imaging results could improve 80% when high order aberrations were introduced, without adding or upgrading hardware. It has significant meaning in promoting the application of LC AO in ground-based large aperture telescopes for visible imaging.

Funding

National Natural Science Foundation of China (NSFC) (61805238).

Acknowledgments

This work is supported by CAS Interdisciplinary Innovation Team and State Key Laboratory of Applied Optics, Changchun Institute of Optics, Fine Mechanics and Physics, Chinese Academy of Sciences.

References

1. L. M. Close, "A review of astronomical science with visible light adaptive optics," Proc. SPIE **9909**, 99091E (2016).
2. C. Baranec, R. Riddle, N. M. Law, A. N. Ramaprakash, S. Tendulkar, K. Hogstrom, K. Bui, M. Burse, P. Chordia, and H. Das, "Rise of the machines: first year operations of the Robo-AO visible-light laser-adaptive optics instrument," presented at the *Proceedings of the Advanced Maui Optical and Space Surveillance Technologies Conference*, Wailea, Maui, Hawaii, 10–13 Sept. 2013.
3. T. Fusco, J. F. Sauvage, D. Mouillet, A. Costille, C. Petit, J. L. Beuzit, K. Dohlen, J. Milli, J. Girard, and M. Kasper, "SAXO, the SPHERE extreme AO system: on-sky final performance and future improvements," Proc. SPIE **9909**, 99090U (2016).
4. C. Boyer and B. Ellerbroek, "Adaptive optics program update at TMT," Proc. SPIE **9909**, 990908 (2016).
5. A. G. Basden, N. A. Bharmal, R. M. Myers, S. L. Morris, and T. J. Morris, "Monte Carlo simulation of ELT-scale multi-object adaptive optics deformable mirror requirements and tolerances," Mon. Not. R. Astron. Soc. **435**(2), 992–998 (2013).
6. Z. Cao, L. Xuan, L. Hu, Y. Liu, Q. Mu, and D. Li, "Investigation of optical testing with a phase-only liquid crystal spatial light modulator," Opt. Express **13**(4), 1059–1065 (2005).

Optics EXPRESS

7. H. Huang, T. Inoue, and H. Tanaka, "Stabilized high-accuracy correction of ocular aberrations with liquid crystal on silicon spatial light modulator in adaptive optics retinal imaging system," Opt. Express **19**(16), 15026–15040 (2011).
8. Q. Q. Mu, Z. L. Cao, L. F. Hu, Y. G. Liu, Z. H. Peng, L. S. Yao, and L. Xuan, "Open loop adaptive optics testbed on 2.16 meter telescope with liquid crystal corrector," Opt. Commun. **285**(6), 896–899 (2012).
9. Z. Cao, Q. Mu, H. Xu, P. Zhang, L. Yao, and X. Li, "Open loop liquid crystal adaptive optics systems:progresses and results," Hongwai Yu Jiguang Gongcheng **45**(4), 0402002 (2016).
10. F. Feng, I. H. White, and T. D. Wilkinson, "Aberration Correction for Free Space Optical Communications Using Rectangular Zernike Modal Wavefront Sensing," J. Lightwave Technol. **32**(6), 1239–1245 (2014).
11. G. D. Love, "Liquid-crystal phase modulator for unpolarized light," Appl. Opt. **32**(13), 2222–2223 (1993).
12. G. D. Love, S. R. Restaino, R. C. Carreras, G. C. Loos, R. V. Morrison, T. Baur, and G. Kopp, "Polarization insensitive 127-segment liquid crystal wavefront corrector," in *Adaptive Optics, Vol. 13 of 1996 OSA Technical Digest Series* (Optical Society of America, 1996), pp. 288–290.
13. J. E. Stockley, G. D. Sharp, S. A. Serati, and K. M. Johnson, "Analog optical phase modulator based on chiral smectic and polymer cholesteric liquid crystals," Opt. Lett. **20**(23), 2441 (1995).
14. Q. Mu, Z. Cao, D. Li, L. Hu, and L. Xuan, "Open-loop correction of horizontal turbulence: system design and result," Appl. Opt. **47**(23), 4297–4301 (2008).
15. Q. Mu, Z. Cao, L. Hu, Y. Liu, Z. Peng, and L. Xuan, "Novel spectral range expansion method for liquid crystal adaptive optics," Opt. Express **18**(21), 21687–21696 (2010).
16. Z. Cao, Q. Mu, L. Hu, Y. Liu, Z. Peng, Q. Yang, H. Meng, L. Yao, and L. Xuan, "Optimal energy-splitting method for an open-loop liquid crystal adaptive optics system," Opt. Express **20**(17), 19331–19342 (2012).
17. H. Hu, L. Hu, Z. Peng, Q. Mu, X. Zhang, C. Liu, and L. Xuan, "Advanced single-frame overdriving for liquid-crystal spatial light modulators," Opt. Lett. **37**(16), 3324–3326 (2012).
18. D. Y. Li, L. F. Hu, Q. Q. Mu, Z. L. Cao, Z. H. Peng, Y. G. Liu, L. S. Yao, C. L. Yang, X. H. Lu, and L. Xuan, "Wavefront processor for liquid crystal adaptive optics system based on Graphics Processing Unit," Opt. Commun. **316**, 211–216 (2014).
19. T. R. Rimmele, K. Richards, S. Hegwer, G. Moretto, L. V. Didkovsky, C. J. Denker, M. Langlois, and J. Marino, "First results from the NSO/NJIT solar adaptive optics system," Proc. SPIE **5171**(170), 179–186 (2004).
20. C. Rao, L. Zhu, X. Rao, L. Zhang, H. Bao, L. Kong, Y. Guo, L. Zhong, X. A. Ma, M. Li, C. Wang, X. Zhang, X. Fan, D. Chen, Z. Feng, N. Gu, and Y. Liu, "Instrument description and performance evaluation of a high-order adaptive optics system for the 1 m new vacuum solar telescope at Fuxian Solar Observatory," Astrophys. J. **833**(2), 210 (2016).
21. X. Zhang, Z. Cao, H. Xu, Y. Wang, D. Li, S. Wang, C. Yang, Q. Mu, and L. Xuan, "High precision system modeling of liquid crystal adaptive optics systems," Opt. Express **25**(9), 9926–9937 (2017).
22. D. Dayton, S. Browne, J. Gonglewski, and S. Restaino, "Increased bandwidth liquid crystal MEMS adaptive optics system," Proc. SPIE **5572**, 303–309 (2004).